

CMOS-compatible athermal silicon microring resonators

Biswajeet Guha¹, Bernardo B. C. Kyotoku^{1,2} & Michal Lipson¹

¹School of Electrical and Computer Engineering, Cornell University, Ithaca, New York 14853, USA.

²Departamento de Física, Universidade Federal de Pernambuco, Recife, Pernambuco, Brazil.

Silicon photonics promises to alleviate the bandwidth bottleneck of modern day computing systems^{1, 2, 3}. But silicon photonic devices have the fundamental problem of being highly sensitive to ambient temperature fluctuations due to the high thermo-optic (TO) coefficient of silicon ($\sim 1.86 \times 10^{-4} \text{ K}^{-1}$)⁴. Most of the approaches proposed to date to overcome this problem either require significant power consumption or incorporate materials which are not CMOS-compatible. Here we demonstrate a new class of optical devices which are passively temperature compensated, based on tailoring the optical mode confinement in silicon waveguides. We demonstrate the operation of a silicon photonic resonator over very wide temperature range of greater than 80 degrees. The fundamental principle behind this work can be extended to other photonic structures such as modulators, routers, switches and filters.

A passive CMOS-compatible thermal stabilization scheme of resonant photonic devices will go a long way towards enabling the implementation of ultralow power optical interconnects. This is because resonant devices such as microring resonators are ideally suited for dense integration of optical networks due to their compact size, high extinction ratio per unit length, low insertion loss and low power consumption^{5, 6, 7}. But they are also highly sensitive to temperature ($\sim 0.11 \text{ nm/K}$) because of their narrow bandwidth. Typical temperature fluctuations in a commercial microprocessor can be 10s of degrees within a local hotspot⁸, degrading considerably the performance of these resonant devices. Relatively temperature stable structures can in principle be achieved using Mach-Zehnder interferometers; however their power and size are not scalable for dense integration. There has been significant effort in stabilizing these devices by delocalizing the mode and overlaying a polymer coating with a negative TO coefficient^{9, 10, 11}. But polymers are currently not compatible with CMOS process. Another approach is to use local heating of silicon itself to dynamically compensate for

any temperature fluctuations^{12, 13, 14}. However, an active compensation scheme is both cumbersome (requiring thermo electric coolers and controllers) and power hungry.

Here we demonstrate the control of the thermal drift of photonic structures by tailoring the degree of optical confinement in silicon waveguides. The basic photonic structure we propose consists of a ring resonator overcoupled to a balanced Mach-Zehnder interferometer (MZI)¹⁵. The schematic of the device is shown in Fig. 1a. The MZI thermal properties can be tuned by design by varying the waveguide widths in the MZI arms¹⁶, and set to counteract the thermal drift of the ring. This additional degree of freedom in choice of waveguide widths, apart from just the lengths, helps in setting the thermal dependence of the MZI independent of the filter spectral order. The waveguide widths and lengths are chosen in the two arms of the MZI to give a balanced transmission ($\Delta(n \cdot L)_{MZI} = 0$) (see Fig. 1b) while having a strong negative temperature sensitivity overall ($\frac{\partial}{\partial T} \Delta(n \cdot L)_{MZI} < 0$). The ring has a large enough waveguide width to enable highly confined single mode operation, and consequently strong positive temperature sensitivity ($\frac{\partial}{\partial T} \Delta(n \cdot L)_{Ring} > 0$). The relative temperature sensitivities of the ring and the MZI, compared in Fig. 1c, are designed to cancel each other out.

The device is made inherently robust to temperature changes - its resonance oscillate about a central wavelength with temperature instead of drifting away, as is the case in standard resonators, due to the periodic interplay of the ring and MZI phase change with temperature. These oscillations arise due to the difference in the linear phase induced by the MZI with temperature and the nonlinear phase induced by the ring. This phase difference, captured in Eqn. (1), is converted into intensity modulation at the output of the structure.

$$\frac{\partial}{\partial T} \phi_{REMZI}(T) = \frac{\partial}{\partial T} \left\{ \text{phase} \left(\frac{t - \alpha e^{j\beta L_{Ring}(T)}}{1 - \alpha t e^{j\beta L_{Ring}(T)}} \right) \right\} + \frac{\partial}{\partial T} (\beta L_{MZI}(T)) \quad (1)$$

L_{ring} and L_{MZI} are the net optical path lengths for the ring and the MZI respectively, t is the cross coupling coefficient of the ring to waveguide, and $(1 - \alpha)$ is the roundtrip loss in the ring. The first term in Eqn. (1) is the change of phase induced by the ring with temperature, which redshifts the resonance with increase in temperature; while the

second term refers to the change in optical path lengths of the two arms of the MZI with temperature designed to have a strong negative value, which compensates for the phase change of the ring. The difference in these phases can be seen in Fig. 2a where we plot, as an example, the phase change at a given wavelength of a 40 μm radius ring resonator as a function of temperature, and the phase added of the MZI at that wavelength. In all our simulations, we used thermo-optic coefficient of silicon as $1.86 \times 10^{-4} \text{ K}^{-1}$ and that of oxide as $1 \times 10^{-5} \text{ K}^{-1}$. It can be seen that the nonlinearity of the ring phase gives rise to two distinct regions – one where the MZI added phase is smaller than the compensating phase required, and one where the MZI added phase is larger than the compensating phase required. The corresponding resonance lineshapes at each of these temperature ranges is shown in Fig. 2b. For a temperature change of T_{per} from base temperature, the resonance lineshape exactly corresponds to the one initially; hence T_{per} is one temperature cycle within which the resonance undergoes a complete oscillation as shown in Fig. 2b. It is this periodic mismatch between the phase added by the MZI and the phase compensation required that gives rise to oscillation in the ring resonance with temperature.

For a ring of given radius, only a particular choice of compensating MZI can result in perfect oscillations in the ring resonance with temperature. If the compensation is too large or too small, the ring resonance drifts away with increase of while still exhibiting the periodic behaviour. This is in sharp contrast with normal ring resonator systems, where the resonance drifts monotonically with temperature. The locus of minima points of the spectra for such a system varies with temperature as

$$\Delta\lambda_{\min} = \left(\frac{\lambda_0}{L_{\text{Ring}} + \chi L_{\text{MZI}}} \right) \frac{\partial L_{\text{Ring}}}{\partial T} \left\{ T - \frac{2}{\beta \frac{\partial L_{\text{Ring}}}{\partial T}} \tan^{-1} \left\{ \frac{1-t}{1+t} \tan \left(\frac{\gamma \beta \frac{\partial L_{\text{Ring}}}{\partial T} T}{2} \right) \right\} \right\} \quad (2)$$

where $\chi = \frac{1-t^2}{1+t^2 + 2t \cos(\beta L_{\text{MZI}})}$ and $\gamma = \frac{\partial L_{\text{MZI}}}{\partial T} / \frac{\partial L_{\text{Ring}}}{\partial T}$ is the compensation factor. Fig. 3a

shows the behaviour of $\Delta\lambda_{\min}$ for different cases of compensating factor (γ). Only when $\gamma = 1$, we get perfect oscillations in the resonance minima with temperature. If $\gamma > 1$, the ring is overcompensated and the resonance slowly blueshifts with temperature; while if

$\gamma < 1$, the ring is undercompensated and the resonance slowly redshifts. For reference $\Delta\lambda_{\min}$ shift with temperature for a normal uncompensated ring resonator is also shown in Fig. 3a, which increases monotonically with temperature.

Smaller oscillations with temperature can be achieved by using structures where the phase compensation mismatch is smaller. This can be achieved using a structure with a large radius (see Fig. 3b). Since the resonances of a larger ring are closely spaced, the phase compensation mismatch width (shown in Fig. 2a) is smaller. Smaller oscillations can also be achieved using N smaller rings with radii $R \pm \delta r$ stabilized using one MZI (for WDM (wavelength division multiplexing) systems¹⁷). From Eqn. (2), it can be deduced that the resulting thermal oscillations ($\Delta\lambda_{\min}$) will be $1/N$ times smaller than single ring case.

Devices were fabricated on a silicon-on-insulator (SOI) wafer with 240 nm Si thickness and 3 μm buried oxide thickness using electron-beam lithography. Fig. 4a shows the optical microscope image of a 40 μm radius ring resonator coupled to a balanced MZI, with SEM insets showing the corresponding waveguide widths. The wide and narrow waveguide widths were measured to be 420 nm and 190 nm respectively. The waveguides taper over a length of 10 μm at the width transition regions. The ring-to-waveguide coupling gap was 110 nm for this specific device. The lengths of the MZI arms are also shown in Fig. 4a. The measured quality factor of the ring was around 7000, a good value for switching and modulating applications for up to 10Gbps input data¹⁸. Quality factor is defined for the case when the spectral shape is perfect lorentzian (see Fig. 2c, $T=T_{per}$).

The fabricated devices show temperature stability over a large temperature range of over 80K. Transmission spectra of this device was measured at different temperatures, and then overlaid together to confirm the oscillating resonance behaviour. The transmission around 1565.5 nm for several different temperatures is shown in Fig 4b, with arrows showing athermal wavelengths λ_{high1} , λ_{high2} and λ_{low} . This behaviour is exhibited for all the resonances in the spectrum over a 100 nm bandwidth. In this particular case the oscillation in transmission minima was less than 1 nm. We also measured less than 3 dB degradation in the extinction ratio between the transmission at the resonance HIGH (λ_{high1} and λ_{high2}) and at the resonance LOW (λ_{low}) value.

Continuous operation over 80 degrees (20 °C to 100 °C) was demonstrated by passing a 1 Gbps, 2^7 -1 pseudo-random data at a bar port resonance. The transmission wavelength was chosen slightly off-resonance (Fig. 4c inset) since the spectral shape at base temperature (22.5 C) was not perfectly lorentzian. Eye patterns were obtained at different temperatures and the relative degradation in eye opening (normalized to starting temperature) is shown in Fig 4c. The corresponding eye diagrams show error free operation over the entire range. The eye opening decreases and increases with temperature as expected due to the oscillatory behaviour of the structure. The eye never closes goes below 3 dB relative to the base temperature, thus proving athermal-like behaviour.

In summary, we have demonstrated for the first time a temperature insensitive resonator-based device on silicon, with no extra power required for thermal stabilization. The device is shown to operate over a wide temperature and spectral range. The device is expected to have high performance as long the dielectric refractive indices change linearly with temperature. It is also assumed that both the ring and the MZI are located in the same thermal hotspot which is typically $500 \times 500 \mu\text{m}^2$ in commercial microprocessors⁸. The approach presented here can be used in a ring resonator modulator system by surrounding the ring with diodes. A reduction in footprint of the device could be achieved by using narrower waveguides in MZI arm, or routing the arms in a coiled manner. The performance of the device could be further enhanced by using splitters/ couplers which are refractive index independent (like Y-splitters). This new generation of devices could lead to ultralow power on-chip optical interconnects capable of meeting the demands for the next generation of microprocessors.

References

- ¹ Miller, D. A. B. Rationale and challenges for optical interconnects to electronic chips, *Proc. IEEE* **88**, 728-749 (2000).
- ² Alduino, A. and Paniccia, M. Interconnects - Wiring electronics with light, *Nature Photon.* **1**, 153-155 (2007).
- ³ Kimerling, L. C. Photons to the rescue: Microelectronics becomes microphotonics, *Electrochemical Society Interface* **9**, 28-31 (2000).

- 4 Varshni, Y. P. Temperature dependence of the energy gap in semiconductors, *Physica (Amsterdam)* **34**, 149-154 (1967).
- 5 Lipson, M. Compact Electro-Optic Modulators on a Silicon Chip, *IEEE J. Sel. Top. Quant. Electron.* **12**, 1520-1526 (2006).
- 6 Xu, Q. F., Schmidt, B., Pradhan, S., and Lipson, M. Micrometre-scale silicon electro-optic modulator, *Nature* **435**, 325-327 (2005).
- 7 Baehr-Jones, T. et al. Optical modulation and detection in slotted silicon waveguides, *Opt. Express* **13**, 5216-5226 (2005).
- 8 Mesa-Martinez, F. J., Brown, M., Nayfach-Battilana, J., and Renau, J. Measuring power and temperature from real processors, *IEEE International Symposium on Parallel and Distributed Processing*, Miami, FL, 2008.
- 9 Alipour, P., Hosseini, E. S., Eftekhari, A. A., Momeni, B., and Adibi, A. Temperature-Insensitive Silicon Microdisk Resonators Using Polymeric Cladding Layers, *Conference on Lasers and Electro-Optics (CLEO)*, Baltimore, MD, 2009.
- 10 Han, M. and Wang, A. Temperature compensation of optical microresonators using a surface layer with negative thermo-optic coefficient, *Opt. Lett.* **32**, 1800-1802 (2007).
- 11 Teng, J. et al. Athermal Silicon-on-insulator ring resonators by overlaying a polymer cladding on narrowed waveguides, *Opt. Express* **17**, 14627-14633 (2009).
- 12 Amatya, R. et al. Low Power Thermal Tuning of Second-Order Microring Resonators, *Conference on Lasers and Electro-Optics/ Quantum Electronics and Laser Science Conference and Photonic Applications Systems Technologies*, Baltimore, MD, 2007.
- 13 Manipatruni, S. et al. Wide temperature range operation of micrometer-scale silicon electro-optic modulators, *Opt. Lett.* **33**, 2185-2187 (2008).
- 14 Watts, M. R. et al. Adiabatic Resonant Microrings (ARMs) with Directly Integrated Thermal Microphotronics, *Conference on Lasers and Electro-Optics (CLEO)*, Baltimore, MD, 2009.
- 15 Absil, P. P., Hryniewicz, J. V., Little, B. E., and Wilson, R. Compact microring notch filters, *IEEE Photon. Technol. Lett.* **12**, 398-400 (2000).
- 16 Uenuma, M. and Moooka, T. Temperature-independent silicon waveguide optical filter, *Opt. Lett.* **34**, 599-601 (2009).
- 17 Manipatruni, S., Chen, L., and Lipson, M. 50 Gbit/s WDM modulation capacity on Silicon, presented at the *Group 4 Photonics*, San Francisco, 2009.
- 18 Lee, B. G., Small, B. A., Bergman, K., Xu, Q., and Lipson, M. Transmission of high-data-rate optical signals through a micrometer-scale silicon ring resonator, *Opt. Lett.* **31**, 2701-2703 (2006).

Acknowledgements This work was performed in part at the Cornell Nano-scale Science & Technology Facility (a member of the National Nanofabrication Users Network) which is supported by National

Science Foundation (Grant ECS-0335765), its users, Cornell University and Industrial Affiliates. We would also like to acknowledge the support of the National Science Foundation's CAREER Grant No. 0446571, as well as the Interconnect Focus Center Research Program at Cornell University, supported in part by Micro-Electronics Advanced Research Corporation (MARCO). The authors would also like to thank S. Manapatruni and L. Chen for helpful discussions.

Author Contributions B.G. designed fabricated and tested the devices. B.B.C.K. helped in the testing. B.G., B.B.C.K. and M.L. discussed the results and their implications and contributed to writing this manuscript.

Author Information Correspondence and requests for materials should be addressed to M.L. (ml292@cornell.edu).

Figure 1 a, Schematic of the device showing the various waveguide lengths and widths. The MZI is highlighted in blue and the ring in red. **b**, Typical transmission spectrum for such a device with 40 μm ring radius and the MZI is balanced, i.e. the overall path lengths of the two arms are equal. **c**, Change in optical path length with temperature for the ring and MZI. The devices are designed to have opposite and equal phase shifts with increase in temperature.

Figure 2 a, Phase change induced by in ring and by the MZI with temperature. The inherent nonlinearity in the ring phase gives rise to distinct overcompensated and uncompensated regions. This behaviour repeats itself after one temperature period T_{per} . **b**, Corresponding resonance lineshapes at different temperatures within one temperature period. The resonance displays periodic oscillations centred at $\lambda = \lambda_{\text{res}}$.

Figure 3 a, Resonance minima shift for different cases of compensation for a ring resonator with 40 μm radius, showing the oscillatory behaviour with temperature. The monotonic drift of an uncompensated ring is also added for reference. **b**, Resonance minima shift with temperature for different ring resonator radii. The resonances oscillate less for larger rings, as compared to smaller rings.

Figure 4 a, Optical microscope image of the device consisting of a 40 μm radius ring resonator coupled to a MZI whose lengths are shown. The coupling gap is 110 nm. SEM insets show the actual waveguide widths at various parts of the device. **b**, Transmission spectrum of the device, centred around 1565.6 nm, taken at different temperatures. The 'athermal wavelengths' are marked as λ_{high1} , λ_{high2} and λ_{low} . The worst case degradation at these wavelengths is less than 3 dB. **c**, Peak-to-peak value in the eye patterns at different temperatures, normalized to the value at base temperature (22.5 $^{\circ}\text{C}$).

The probe wavelength was 1542.375 nm, shown in the inset. The degradation in the eye opening was less than 3 dB over a range of 80 degrees.

Figure 1

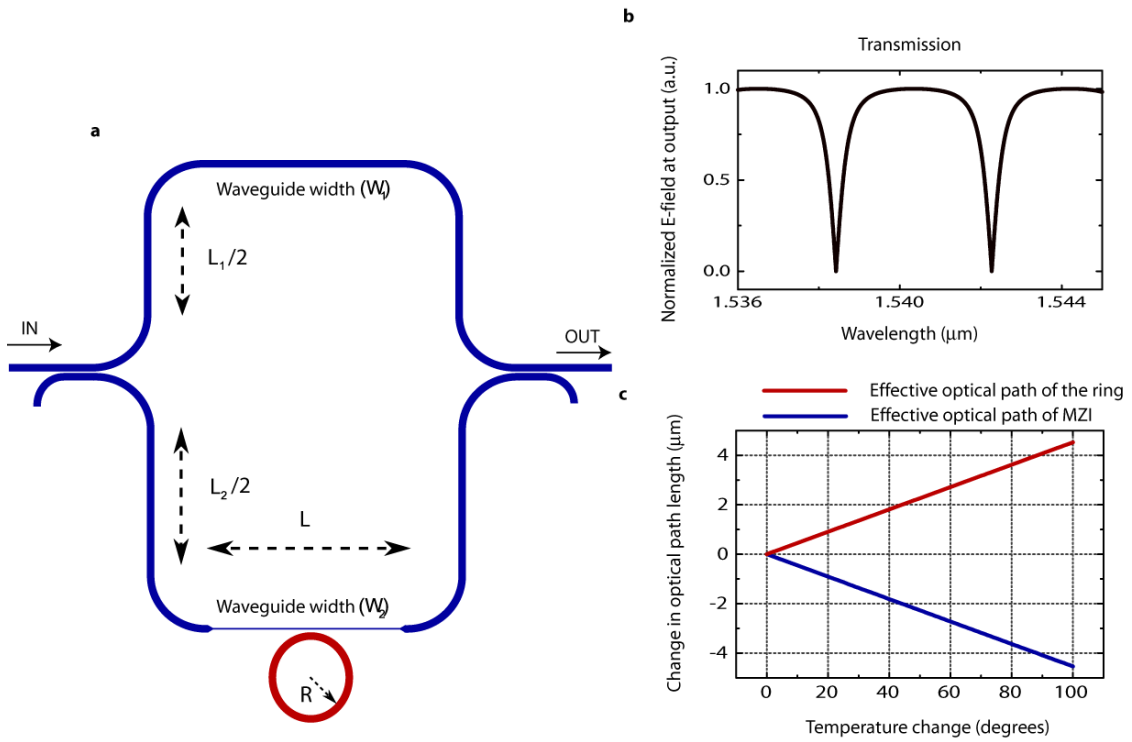


Figure 2

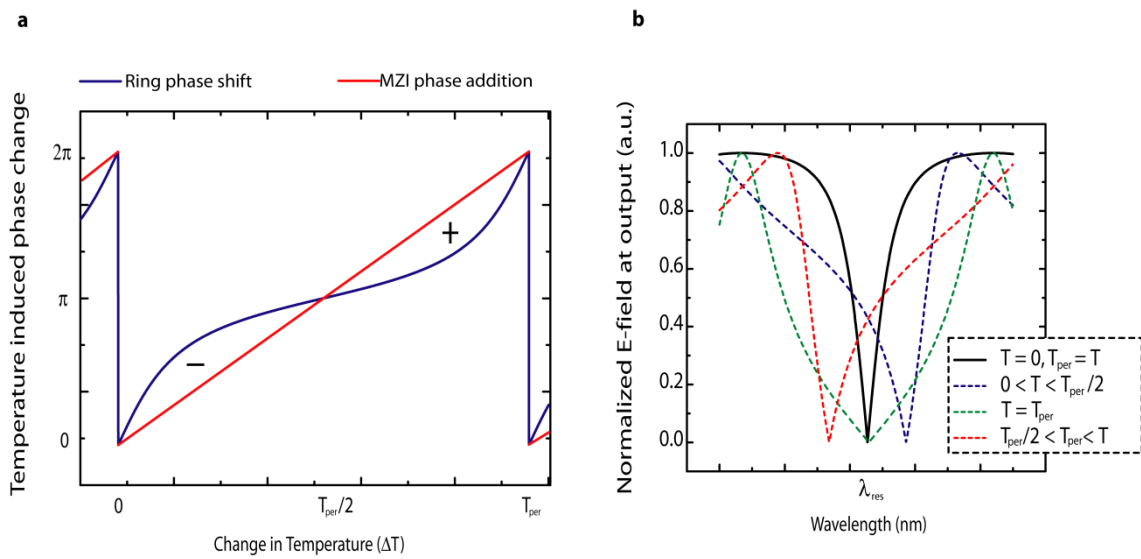


Figure 3

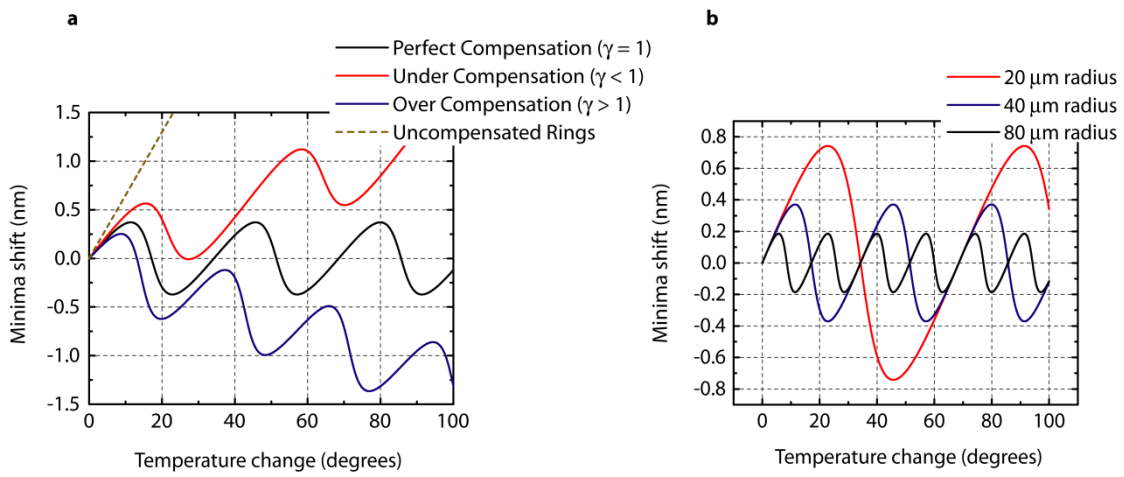


Figure 4

